RSC Advances

PAPER

View Article Online
View Journal | View Issue

Cite this: *RSC Adv.*, 2015, **5**, 68579

Air-stable PbS quantum dots synthesized with slow reaction kinetics *via* a $PbBr_2$ precursor

Lin Yuan,[a] Robert Patterson,[a] Wenkai Cao,[a] Zewen Zhang,[a] Zhilong Zhang,[a] John A. Stride,[b] Peter Reece,[c] Gavin Conibeer[a] and Shujuan Huang*[a]

PbS quantum dots have been synthesized using a $PbBr_2$ precursor and the halide content has been examined. Slower reaction kinetics for quantum dots growth relative to the use of $PbCl_2$ was observed for $PbBr_2$, giving a possible route to increased control over quantum dot size with *in situ* passivation. Unambiguous determination of the surface conditions of nanomaterials is still a developing area of science, pushing the limits of current microscopy and analytical techniques. Contributions to a rigorous form of nanomaterial surface analysis are made here using X-ray photoelectron spectroscopy to analyse bonding in detail. Atomic resolution TEM is applied to produce energy dispersive X-ray spectroscopy maps with state of the art resolution. This analysis has been applied to air-stable halide terminated PbS nanoparticles, which is a nanomaterial of central importance for quantum confined solar cell applications. Chemical analysis from X-ray photoelectron spectroscopy is consistent with Br surface termination and high resolution energy dispersive X-ray spectroscopy (EDS) maps also show a positive spatial correlation for Br with quantum dot location. An observed excess Br content is attributed to the presence of bromine terminated PbS quantum dots nuclei in the final colloid.

Received 10th July 2015
Accepted 3rd August 2015

DOI: 10.1039/c5ra13499d

www.rsc.org/advances

Introduction

Semiconductor nanoparticles, sometimes as quantum dots (QDs), fabricated from lead chalcogenides are central to a number of advanced concepts in nanotechnology. PbS QDs have been used as a sensitizer and a light absorbing material in solar cells.[1] Perhaps most notable is the advantageous application of quantum confined PbS QDs in the area of colloidal quantum dot solar cells.[2,3] The first PbS quantum dot solar cell was fabricated in 2005.[4] An efficiency greater than 1% was achieved in 2008 using a Schottky structure.[5] Over the past three years, efficiencies in these cells have climbed steadily,[6–9] with the record efficiency currently standing at 9.2%.[10] This suggests that there is substantial potential for these materials to produce low cost solution-processed solar cells employing novel quantum confinement effects. In addition, these nanomaterials offer avenues for possibly fabricating hot carrier (HC) and multiple exciton generation devices.[11–13]

Synthesis of colloidal PbS quantum dots has been performed extensively and PbS colloidal synthesis recipes are increasingly mature.[14,15] With the substantial interest in quantum confinement effects, tunable bandgaps and modified photonic and phononic properties for photovoltaic and photonic applications, synthesis recipes for PbS quantum dots continue to be of significant interest. PbS quantum dots can be synthesized with a number of different lead chemical precursors. The choice of chemical precursor has been shown to be important with the discovery of halide atomic ligand surface passivation offered by synthesis with Pb–halide precursors instead of a PbO precursor.[16–18] The presence of halide atoms on the surface of the quantum dots has generally been inferred from the impressive air stability of these materials.[19,20] However, these current methods have some disadvantages, such as the use of expensive TMS_2S, the difficulties in synthesizing small particles with *in situ* passivation, or the requirements for large quantities of chemicals.

Synthesis with halide precursors comes with a few practical concerns, such as the removal of the unreacted portion of the commonly used Pb precursor from the PbS precipitate. Methods to address this have been demonstrated in the literature and continue to be developed. The level of residue can be assessed using conventional TEM where small (~1 nm) unreacted PbX_2 (X = Cl, Br) particles are generally visible. Residue below the level of visible particulates is also generally difficult to assess.

Synthesis of halide-terminated nanoparticles has been performed recently, as well as nanoparticles that have multiple ligands.[17] This trend toward increasingly complex surface terminations has potential to continue. However it is still very difficult to unambiguously assess the surface chemistry of nanomaterials, this article contributes to a methodology for more unambiguous determination of the surface chemistry of

[a]*School of Photovoltaic and Renewable Energy Engineering, The University of New South Wales, Sydney 2052, Australia. E-mail: sj.huang@unsw.edu.au*
[b]*School of Chemistry, The University of New South Wales, Sydney 2052, Australia*
[c]*School of Physics, The University of New South Wales, Sydney 2052, Australia*

PbS quantum dots fabricated from a $PbBr_2$ precursor. The growth rates for particles using the $PbBr_2$ and $PbCl_2$ precursors were assessed and a measurable difference observed, with synthesis using the $PbBr_2$ precursor yielding approximately 30% smaller quantum dots with surface passivation under the same reaction conditions as that for the $PbCl_2$ precursor. It was of interest to determine the actual bromine content of the system and to attempt to determine the spatial dependence of the bromine distribution. Strong correlations of bromine content to the quantum dot locations would be expected for bromine surface termination. X-ray Photoelectron Spectroscopy (XPS) was used to assess both the content and bonding nature of the bromine in the nanomaterials. energy dispersive X-ray spectroscopy (EDS) was also used to map the spatial distribution of bromine using atomic resolution TEM.

Results and discussion

Recently Weidman and co-workers have reported that a large excess of $PbCl_2$ precursor (Pb : S ratio of 24 : 1) results in the formation of highly monodisperse PbS quantum dots due to the delaying of the onset of Ostwald ripening.[16] In this work, a much smaller $PbBr_2$ precursor to sulphur (Pb : S) ratio of 4 : 1 was used. The primary interest in the work was to attempt to track the location and concentration of any halides in the system in the final washed material rather than maximize a monodisperse particle size. Nonetheless, the degree of monodispersity offered by the 4 : 1 precursor ratio was sufficient for this. The dependence of growth rates of the PbS quantum dots as a function of the reaction conditions was studied. PbS quantum dots were synthesized by using $PbBr_2$ at three different, 80 °C, 120 °C and 160 °C, $PbCl_2$ was used at 80 °C as a reference.

Fig. 1 shows the transmission electron microscopy (TEM) images as well as a histogram of the sizes of the PbS quantum dots synthesized. The size has been estimated by measuring more than a hundred nanoparticles in the high resolution images. Compared to the quantum dots synthesized *via* $PbCl_2$ as shown in Fig. 1(a), quantum dots synthesized using $PbBr_2$ (Fig. 1(b)) were observed to have approximately a 30% smaller diameter than that from $PbCl_2$ under the same reaction conditions, *i.e.* 80 °C for 1 min. Fig. 2(a) shows a dramatic blue shift from 1336 nm to 954 nm in the absorbance peak of PbS quantum dots when changing the lead precursor from $PbCl_2$ to $PbBr_2$, corresponding to an approximate size decrease from 5.7 to 4.1 nm according to Weidman's model.[16] This suggests that the reaction *via* the $PbBr_2$ is slower so as to suppress Ostwald ripening and to provide better control on quantum dot synthesis, particularly promising for ultra-small wide bandgap quantum dots.

By using the "hard–soft acid–base" theory,[21] we can explain this phenomenon. According to this theory, "soft" acid can bind with "soft" base easier than "hard" base, and Pb is a kind of "soft" acid, while Br is a "softer" base than Cl, so Pb–Br bond requires higher energy to be break which leads to a much slower reaction speed and longer nuclei period.

Higher temperatures for hot injection result in larger quantum dots as shown in Fig. 1(b)–(d), as expected. The resulting quantum dot sizes are listed in Table 1. From high-resolution TEM (HRTEM) imaging lattice fringes were observed suggesting that the quantum dots are highly crystalline.

Smaller quantum dots were fabricated using a shorter reaction time, *i.e.* 10 s at different temperatures. The smallest size obtained was 2.9 nm, which was synthesized at 80 °C for 10 s.

Fig. 2(b) shows well-defined absorption peaks from 878 nm to 1336 nm. The quantum dot size has been estimated using the model proposed by Weidman. As shown in Table 1, these estimates are in good agreement with the sizes measured from TEM images. These quantum dots have shown strong PL emission. A PL spectrum of the PbS synthesized at 120 °C for 1 min is shown in Fig. 2(b) inset. The Stoke shift of PL peak from the absorbance is ~150 nm which is consistent to other published work. Also a 190 nm full width at half max (FWHM), very similar to that of the absorbance peak, indicates a good size distribution of quantum dot size.

We have evaluated the crystallinity and purity of the quantum dots by X-ray diffraction (XRD). Fig. 3 shows the XRD pattern of the quantum dots after five washes. The peaks match with the PbS rock salt crystalline structure (ICDD PDF number 00-005-0592). There is no additional peak observed from the sample, which suggests that the unreacted $PbBr_2$ residue was removed effectively. The typical fringe spacings measured from the high resolution TEM images are 3.0 and 3.5 Å, which correspond to the {200} and {101} lattice planes of the rock salt structure PbS, respectively.

The air stability of the PbS quantum dots (synthesized at 120 °C for 1 min) was assessed under ambient conditions for over one month and the change in the position of absorbance peak was measured. From Fig. 4, there was no observable shift between peaks measured at different times, indicating that the quantum dots were stable against ambient oxygen due to passivation of Pb atom with stable Br atoms. Similar work using $PbCl_2$ precursor has been demonstrated by Weidman.[16]

The other advantage of using halide atom to passivate quantum dot surface is a higher quantum yield can be obtained. These halide atoms can be expected to bind with Pb atoms, where the risk of oxidation is high. By reducing the exposed surface, the halide passivated PbS quantum dots could achieve a higher quantum yield.[17] Moreover, oleic acid ligand may be removed during the washing process while halide atoms can still bind with quantum dots.[7]

Having obtained bromine terminated PbS quantum dots, it was of interest to obtain more information about the physical and chemical environment of the halide atoms after the application of the established washing procedure. While halide surface passivation can be inferred from air stability measurements such as those shown in Fig. 4, establishing precedents for more directly probing the halide content would be of substantial utility, particularly as nanomaterials are being fabricated with increasingly complex surface terminations.

XPS measurements were performed on thin films of the Br-terminated PbS quantum dots and analyzed in some detail to obtain information about the relative content and bonding of the halide ions. Fig. 5(a)–(c) show the high-resolution XPS

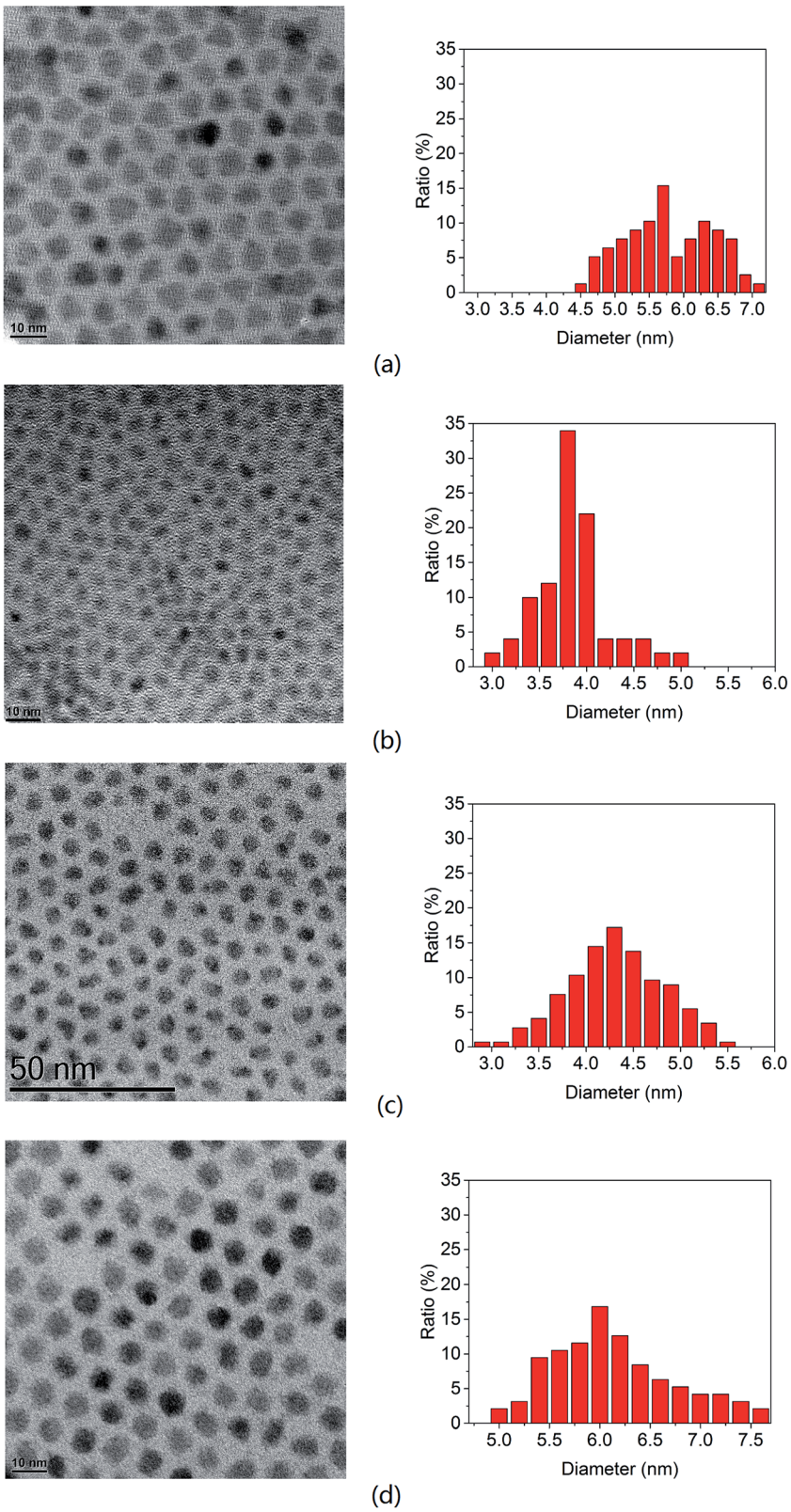

Fig. 1 TEM images and corresponding normalized size distribution histograms from over 100 PbS quantum dots synthesized *via* different precursor and reaction time: (a) $PbCl_2$, 80 °C for 1 min; (b) $PbBr_2$, 80 °C for 1 min; (c) $PbBr_2$, 120 °C for 1 min; (d) $PbBr_2$, 160 °C for 1 min.

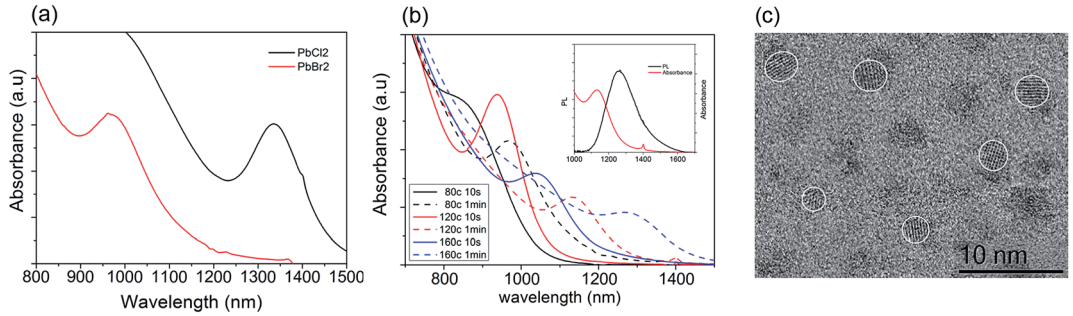

Fig. 2 (a) Comparison of absorbance of PbS quantum dots synthesized *via* $PbBr_2$ and $PbCl_2$ precursor under same condition (80 °C, 1 min). (b) Absorbance of PbS quantum dots synthesized *via* $PbBr_2$ under different conditions, the inset shows PL and absorbance spectrum of PbS QDs which was synthesized at 120 °C for 1 min. (c) HRTEM image of PbS QDs which were synthesized at 80 °C for 10 s, the image shows a clear fringe which indicates a high crystallinity.

spectra of S 2p, Br 3d, and Pb 4f peaks respectively of PbS quantum dots synthesized at 120 °C for 1 min. The S 2p peak at 163.5 eV corresponds to the binding energy of Pb–S while the Br 3d at 68.6 eV corresponds to the binding energy of Br with Pb.[22,23] Both of the fitted peaks clearly show large splitting due to spin orbit coupling. The Pb 4f signal contains two peaks corresponding to the spin orbit interactions for the $4f_{7/2}$ and $4f_{5/2}$ core electronic states. They are clearly both broad and asymmetric, with shoulders corresponding to peak splitting due to perturbations from the local chemical bonding. The $4f_{7/2}$ peak was fitted with two components centred at 137.5 eV and 138.5 eV. The former corresponds to the binding energy of Pb–S, the latter corresponds to Pb–Br bonds. The bonds of Pb and oleic acid ligands may also contribute to the peak at 138.5 eV.[22]

XPS measurements have been used to positively correlate the presence of certain species on the surface of quantum dots. The spectra shown in Fig. 5 are consistent with Br surface termination. However, while XPS can show that lead is bonded to sulphur as well as bromide in the system, it cannot determine whether or not the Pb–Br bond is at the surface of the nanomaterial or whether it appears as a result of $PbBr_2$ residue. Additionally, the XPS analysis indicates an excess of Br in the quantum dot films. The ratio of Pb atoms on the surface to that of the core of an approximately 4.7 nm PbS quantum dot is about 0.56. The ratio of Pb atoms bonded to bromine/oleic acid to those bonded to sulphur obtained from the XPS spectra is 0.66, which is slightly larger than the ratio of 0.56 expected ideally from the PbS quantum dots terminated by Br and oleic acid. This suggests that after an acceptable washing procedure and in the absence of $PbBr_2$ clusters any Br content outside the quantum dots is at very low level.

To complement the XPS analysis, high-resolution EDS mapping has been performed using a large area JEOL Centurio SDD EDS detector that allows elemental mapping with atomic resolution. Probing the precise surface chemistry of nanomaterials is generally quite difficult. Here an attempt is made to do this with reasonable resolution by taking advantage of the atomic resolution available in this particular TEM. Fig. 6 shows a dark-field scanning TEM (STEM) image PbS quantum dots and the corresponding maps of S, Pb, and Br. As suggested by the EDS maps, the positions of S, Pb and Br atoms are highly localized to individual pixels and have significant overlap with the dark field STEM image of the PbS quantum dots.

Pixel by pixel analysis of normalized EDS images was performed using the OpenCV image processing library. By masking 44 of the quantum dots occupying 39% of the image, the relative elemental compositions and their spatial overlap were assessed both inside and outside the quantum dots. Pb and S signals from inside the quantum dot regions being 66% and 70% respectively, consistent with a slight excess of S in the material leading to as-grown p-type doping. The Br signal is flatter, with a measured 57% of the signal coming from the quantum dot regions.

Table 1 Estimated quantum dot mean diameter for different synthesis condition

Synthesis condition	Absorption peak (nm)	Corresponding bandgap (eV)	Estimated size by absorbance (nm) (Weidman model)	Size measured by TEM with 1σ uncertainty (nm)
$PbBr_2$ 80 °C 10 s	~858	1.44	3.7	2.9 ± 0.4
$PbBr_2$ 80 °C 1 min	954	1.30	4.1	4.0 ± 0.4
$PbBr_2$ 120 °C 10 s	938	1.32	4.0	3.9 ± 0.3
$PbBr_2$ 120 °C 1 min	1130	1.10	4.8	4.4 ± 0.5
$PbBr_2$ 160 °C 10 s	1036	1.20	4.4	4.3 ± 0.5
$PbBr_2$ 160 °C 1 min	1266	0.98	5.4	6.2 ± 0.6
$PbCl_2$ 80 °C 1 min	1336	0.93	5.7	5.7 ± 0.6

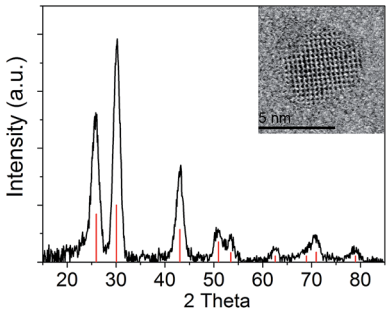

Fig. 3 XRD pattern of PbS quantum dots synthesized *via* $PbBr_2$. The red bars are the reference pattern of PbS rock salt structure (ICDD-5-0592). The inset is HRTEM image of PbS quantum dot which was synthesized at 160 °C for 10 s.

Careful visual inspection of the dark-field HRTEM image shows very small crystallites outside what are nominally the PbS quantum dots that are not readily apparent in bright field images. The rms value of the product of the signal strength at each pixel in two normalized EDS maps for different elements was summed and used as an index to compare elemental spatial overlap. The index ranges from 0 to 1, with 1 obtained from a comparison between identical images. The relative spatial overlap of the elements outside the quantum dot regions was 0.64, 0.4 and 0.63 for Pb–S, Pb–Br and S–Br respectively. The relatively strong correlations between the S and Br elements, as well as Pb and S, outside the quantum dot regions suggests that the signal is coming from something other than $PbBr_2$ residue. Sulphur has high solubility in the solvents used in the washing steps and S content outside the quantum dots is expected to be relatively small.

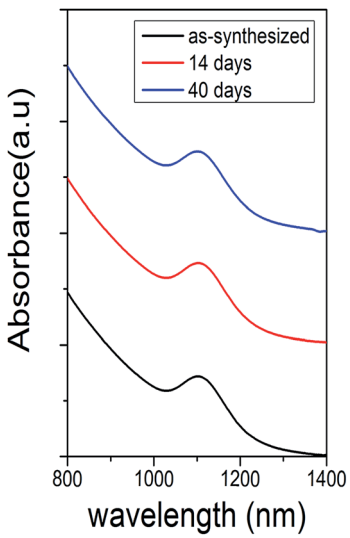

Fig. 4 Absorbance comparison of PbS quantum dots synthesized at 120 °C for 1 min after storage under ambient conditions. There is no observable shift in the absorption peaks over the period of measurement as expected from halide surface passivation. The curves are vertically shifted for the sake of clarity.

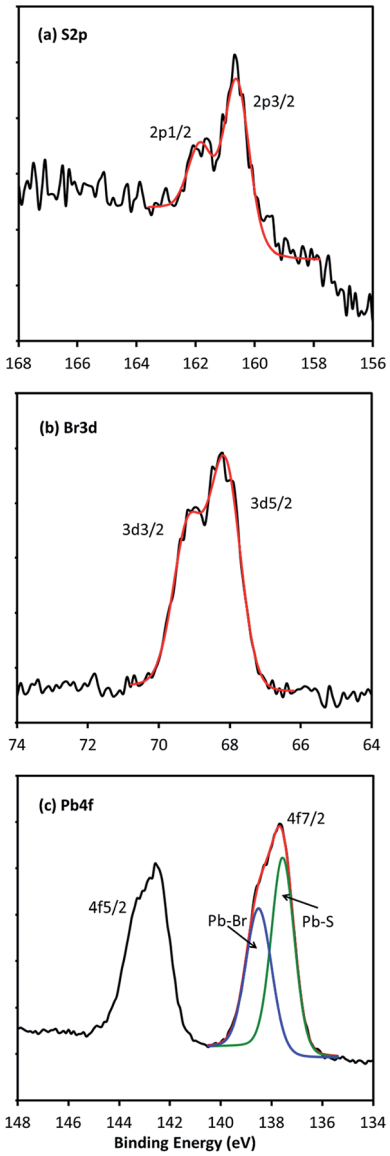

Fig. 5 XPS spectra of PbS quantum dots synthesized at 120 °C for 1 min: (a) S 2p, (b) Br 3d and (c) Pb 4f. All spectra show corresponding peak doublets from spin orbit coupling. The peak for the Br $3d_{5/2}$ state at 68.6 eV corresponds to Br bound to Pb. The Pb $4f_{7/2}$ peak shows further decomposition into two peaks as a result of perturbations to the core electronic states from the bonding of Pb to S and Pb to Br and oleic acid ligands.

From the lightly higher than expected Br content of the quantum dot films measured by XPS and the spatial correlation between Pb and S as well as Br and S outside of the quantum dot regions observed in the EDS maps, we conclude that the small crystallites apparent in the dark field HRTEM image are nuclei of bromine terminated PbS quantum dots. During the growth phase, these nuclei are typically consumed by larger quantum dots. However the 10 second to 1 min reaction times in typical PbS syntheses are relatively short. Unlike precursor chemicals but similar to quantum dots, these nuclei survived the washing procedure and were present in the final colloid. These nuclei would have surface area to volume ratios that are quite large,

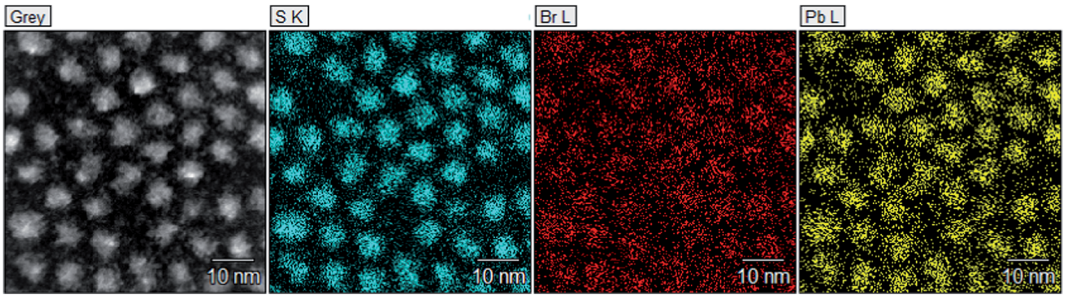

Fig. 6 A dark-field STEM image and the corresponding atomic resolution EDS maps of PbS quantum dots synthesized using a $PbBr_2$ precursor (120 °C, 1 min). Each pixel in each of the maps corresponds to an area of approximately 9 $Å^2$.

leading to higher Br to Pb and S ratios consistent with that observed in XPS. Equivalently these nuclei can be thought of as partially reacted non-stoichiometric atomic clusters that could easily contain increased Br content relative to crystalline PbS quantum dots.

Conclusion

The synthesis *via* $PbBr_2$ precursor has showed observably slower growth rates leading to quantum dots of smaller size relative to those made using $PbCl_2$ precursor. We attribute this to the higher Pb–Br bonding energy according to "hard–soft acid–base" theory. This can lead to increased control over the size of particles without any loss of passivation. The XPS and EDS analysis of PbS quantum dot surfaces yields information on the halide content and location in substantial detail after the quantum dots have been subjected to the thorough washing process required to remove Pb–halide precursors. Nuclei of bromine terminated PbS quantum dots are observed in dark field HRTEM images and indicate an excess Br content confirmed by both the XPS and EDS measurements. Given the impressive air-stability of halide terminated Pb chalcogenide quantum dots, increased understanding of the halide incorporation is bound to be an important aspect of applications of these materials to next-generation photovoltaic cells.

Methods

In a typical synthesis of PbS quantum dots synthesized *via* $PbBr_2$, 1.5 mmol (564 mg) of $PbBr_2$ (Sigma Aldrich, 98%) was mixed with 7.5 ml oleylamine in a three-necked flask, then heated to 120 °C under N_2 flow after degassing for 20 min. 0.375 mmol (12 mg) of sulphur was mixed with 2.25 ml oleylamine, heated to 120 °C under N_2 flow and kept at this temperature for 20 min before being cooled to room temperature. The Pb–oleylamine solution was adjusted to the desired temperature and then 2.25 ml of the S–oleylamine solution was injected. The temperature of the solution was maintained for the time desired for the reaction then heating was stopped. The flask was then submerged in a cold water bath to allow the product solution to cool quickly and stop the reaction.

After synthesis, 20 ml ethanol (Sigma Aldrich, 99.8%) was added to the as-synthesized product solution followed by centrifugation to precipitate the particles. After centrifugation, the supernatant was discarded and the precipitate was re-dispersed in 10 ml of hexane (Scharlau, 96%). 2 ml of oleic acid was added to the solution after another centrifugation. The solution was stirred overnight to complete the ligand exchange. After ligand exchange, 40 ml of methanol (RCI Labscan, 99%) was added to precipitate the particles and remove the excess oleic acid. After centrifugation, the supernatant was discarded and the precipitate was re-dispersed by adding 10 ml of hexane. This process was repeated twice. All processes were performed in ambient conditions with centrifugation at 4000 rpm for 3 min.

PbS quantum dots synthesized *via* $PbCl_2$ were made by following recipes which have been published previously by other researchers.[16] In a typical synthesis, 1.5 mmol (417 mg) of $PbCl_2$ (Alfa Aesar, 99%) was mixed with 7.5 ml oleylamine (Sigma Aldrich, 70%) in a three-necked flask. The solution was degassed for 20 min before being heated to 120 °C in nitrogen. 0.375 mmol (12 mg) of sulphur (Sigma Aldrich, 99.5%) was mixed with 2.25 ml oleylamine, heated to 120 °C under N_2 flow and then cooled to room temperature after 20 min. The Pb–oleylamine solution was cooled to 80 °C and 2.25 ml of the S–oleylamine solution was injected. The combined solution was kept at 80 °C for 1 min before quenching the reaction by submerging the flask into a water bath. The washing process and ligand exchange process was same as the process *via* $PbBr_2$ precursor.

Transmission electron microscopy (TEM) was performed on a Phillips CM200 and a JEOL JEM-ARM200F with a voltage of 200 kV. Energy-dispersive X-ray spectroscopy (EDS) was performed on the JEOL JEM-ARM200F TEM using a large area JEOL Centurio SDD EDS detector that allows elemental mapping with atomic resolution. The sample was prepared by drop-casting the quantum dots solution in hexane onto a copper TEM grid with an amorphous carbon support. Analysis of the TEM image and the particle size calculations were performed using ImageJ software.

The absorbance spectra of the PbS quantum dots were measured using a Perkin Elmer LAMBDA 1050 UV-VIS-NIR spectrophotometer. The quantum dots were dispersed in hexane for this measurement.

X-ray diffraction (XRD) was performed on a PANalytical Xpert Materials Research Diffractometer (MRD) with a Cu anode. Samples were prepared by drop-casting the solution of quantum dots in hexane onto a silicon wafer and drying under ambient conditions.

X-ray photoelectron spectroscopy (XPS) was performed on a Thermo Scientific ESCALAB250Xi, with a mono-chromated Al X-ray source. The power was 150 W and spot size was 500 micrometres. Samples were prepared by drop-casting the concentrated quantum dot solution in hexane onto silicon substrates.

Photoluminescence (PL) spectra was detected by an InGaAs photodetector (Electro Optical Systems, IGA-030-E) using a lock-in amplifier (Stanford Research Systems SR510) and optical chopper. The sample solutions in hexane were excited with an argon ion laser (Coherent Innova 70) emitting at a wavelength of 514.5 nm.

Acknowledgements

This work has been supported by the Australian Government through the Australian Research Council (ARC) and the Australian Renewable Energy Agency (ARENA). Responsibility for the views, information or advice expressed herein is not accepted by the Australian Government. We thank to the Electron Microscopy Unit of UNSW for TEM imaging support, to the Electron Microscopy Centre of University of Wollongong and Dr Gilberto Casillas-Garciafor for EDS measurement, to Dr Bill Gong for XPS measurements. Lin Yuan is financially supported by China Scholarship Council and UNSW.

References

1 F. W. Wise, Lead salt quantum dots: the limit of strong quantum confinement, *Acc. Chem. Res.*, 2000, **33**, 773–780.
2 J. Tang and E. H. Sargent, Infrared colloidal quantum dots for photovoltaics: fundamentals and recent progress, *Adv. Mater.*, 2011, **23**, 12–29.
3 I. J. Kramer and E. H. Sargent, The architecture of colloidal quantum dot solar cells: materials to devices, *Chem. Rev.*, 2014, **114**, 863–882.
4 S. A. McDonald, G. Konstantatos, S. Zhang, P. W. Cyr, E. J. Klem, L. Levina and E. H. Sargent, Solution-processed PbS quantum dot infrared photodetectors and photovoltaics, *Nat. Mater.*, 2005, **4**, 138–142.
5 K. W. Johnston, A. G. Pattantyus-Abraham, J. P. Clifford, S. H. Myrskog, D. D. MacNeil, L. Levina and E. H. Sargent, Schottky-quantum dot photovoltaics for efficient infrared power conversion, *Appl. Phys. Lett.*, 2008, **92**, 151115.
6 M. Pouya, J. L. André, R. K. Ahmad, L. Xinzheng, M. A. Michael, M. T. Susanna, H. Sjoerd, L. Anna, N. Zhijun, F. Armin, A. Aram and H. S. Edward, The Donor–Supply Electrode Enhances Performance in Colloidal Quantum Dot Solar Cells, *ACS Nano*, 2013, **7**, 6111–6116.
7 H. I. Alexander, M. T. Susanna, H. Sjoerd, V. Oleksandr, Z. David, D. Ratan, L. Larissa, R. R. Lisa, H. C. Graham, F. Armin, W. K. Kyle, J. K. Illan, N. Zhijun, J. L. André, C. Kang, A. Aram and H. S. Edward, Hybrid passivated colloidal quantum dot solids, *Nat. Nanotechnol.*, 2012, **7**, 577–582.
8 G. I. Koleilat, X. Wang and E. H. Sargent, Graded recombination layers for multijunction photovoltaics, *Nano Lett.*, 2012, **12**, 3043–3049.
9 X. Wang, G. I. Koleilat, J. Tang, H. Liu, I. J. Kramer, R. Debnath, L. Brzozowski, D. A. R. Barkhouse, L. Levina, S. Hoogland and E. H. Sargent, Tandem colloidal quantum dot solar cells employing a graded recombination layer, *Nat. Photonics*, 2011, **5**, 480–484.
10 C.-H. M. Chuang, P. R. Brown, V. Bulović and M. G. Bawendi, Improved performance and stability in quantum dot solar cells through band alignment engineering, *Nat. Mater.*, 2014, **13**, 796–801.
11 J. Y. Kim, O. Voznyy, D. Zhitomirsky and E. H. Sargent, 25th anniversary article: colloidal quantum dot materials and devices: a quarter-century of advances, *Adv. Mater.*, 2013, **25**, 4986–5010.
12 R. Patterson, M. Kirkengen, B. P. Veettil, D. Konig, M. A. Green and G. Conibeer, Phonon lifetimes in model quantum dot superlattice systems with applications to the hot carrier solar cell, *Sol. Energy Mater. Sol. Cells*, 2010, **94**, 1931–1935.
13 L. Peng, J. Tang and M. Zhu, Recent development in colloidal quantum dots photovoltaics, *Frontiers of Optoelectronics*, 2012, **5**, 358–370.
14 L. Cademartiri, E. Montanari, G. Calestani, A. Migliori, A. Guagliardi and G. A. Ozin, Size-dependent extinction coefficients of PbS quantum dots, *J. Am. Chem. Soc.*, 2006, **128**, 10337–10346.
15 M. Iwan, L. Karel, S. Dries, M. David, N. Tom, C. M. José, V. Frank, V. André, D. Christophe, A. Guy and H. Zeger, Size-Dependent Optical Properties of Colloidal PbS Quantum Dots, *ACS Nano*, 2009, **3**, 3023–3030.
16 M. C. Weidman, M. E. Beck, R. S. Hoffman, F. Prins and W. A. Tisdale, Monodisperse, Air-Stable PbS Nanocrystals *via* Precursor Stoichiometry Control, *ACS Nano*, 2014, **8**, 6363–6371.
17 Z. Jianbing, G. Jianbo, M. M. Elisa, M. L. Joseph and C. B. Matthew, Diffusion-Controlled Synthesis of PbS and PbSe Quantum Dots within SituHalide Passivation for Quantum Dot Solar Cells, *ACS Nano*, 2014, **8**, 614–622.
18 M. Yuan, K. W. Kemp, S. M. Thon, J. Y. Kim, K. W. Chou, A. Amassian and E. H. Sargent, High-Performance Quantum-Dot Solids *via* Elemental Sulfur Synthesis, *Adv. Mater.*, 2014, **26**, 3513–3519.
19 Z. Ning, Y. Ren, S. Hoogland, O. Voznyy, L. Levina, P. Stadler, X. Lan, D. Zhitomirsky and E. H. Sargent, All-inorganic colloidal quantum dot photovoltaics employing solution-phase halide passivation, *Adv. Mater.*, 2012, **24**, 6295–6299.
20 J. Tang, K. W. Kemp, S. Hoogland, K. S. Jeong, H. Liu, L. Levina, M. Furukawa, X. Wang, R. Debnath, D. Cha,

K. W. Chou, A. Fischer, A. Amassian, J. B. Asbury and E. H. Sargent, Colloidal-quantum-dot photovoltaics using atomic-ligand passivation, *Nat. Mater.*, 2011, **10**, 765–771.

21 G.-S. Philippe, W. Brian and Y. Dong, Intraband relaxation in CdSe nanocrystals and the strong influence of the surface ligands, *J. Chem. Phys.*, 2005, **123**, 74709.

22 W. E. Morgan and J. R. van Wazer, Binding energy shifts in the X-ray photoelectron spectra of a series of related Group IVa compounds, *J. Chem. Phys.*, 1973, **77**, 964–969.

23 V. I. Nefedov, A comparison of results of an ESCA study of nonconducting solids using spectrometers of different constructions, *J. Electron Spectrosc. Relat. Phenom.*, 1982, **25**, 29–47.